

Berezinskii-Kosterlitz-Thouless Phase Transition in 2D Spin-Orbit Coupled Fulde-Ferrell Superfluids

Yong Xu and Chuanwei Zhang*

Department of Physics, The University of Texas at Dallas, Richardson, Texas 75080, USA

The experimental observation of traditional Zeeman-field induced Fulde-Ferrell-Larkin-Ovchinnikov (FFLO) superfluids has been hindered by various challenges, in particular, the requirement of low dimensional systems. In 2D, finite temperature phase fluctuations lead to extremely small Berezinskii-Kosterlitz-Thouless (BKT) transition temperature for FFLO superfluids, raising serious concerns regarding their experimental observability. Recently, it was shown that FFLO superfluids can be realized using a Rashba spin-orbit coupled Fermi gas subject to Zeeman fields, which may also support topological excitations such as Majorana fermions in 2D. Here we address the finite temperature BKT transition issue in this system, which may exhibit gapped, gapless, topological, and gapless topological FF phases. We find a large BKT transition temperature due to large effective superfluid densities, making it possible to observe 2D FF superfluids at finite temperature. In addition, we show that gapless FF superfluids can be stable due to their positive superfluid densities. These findings pave the way for the experimental observation of 2D gapped and gapless FF superfluids and their associated topological excitations at finite temperature.

PACS numbers: 03.75.Ss, 03.75.Lm, 74.20.Fg

The exotic Fulde-Ferrell-Larkin-Ovchinnikov (FFLO) superfluids [1, 2] with finite center-of-mass momentum Cooper pairing have played a central role in various fields of physics, such as heavy-fermion superconductors [3–5], organic superconductors [6], two-dimensional electron gases [7], and cold Fermi gases [8]. Despite intensive search, no conclusive evidence of FFLO states has been experimentally observed. One challenge comes from the narrow region of the phase diagram where FFLO superfluids exist [9]. This region increases dramatically in lower dimensions [10, 11]. However, owing to thermal fluctuations, low dimensional systems cannot undergo conventional phase transition to a state with long-range order. In particular, in two dimension (2D), the relevant physics is the Berezinskii-Kosterlitz-Thouless (BKT) transition [12, 13] to a state with quasi-long-range order (*i.e.* vortex-antivortex (V-AV) pairs) [14–16], with the critical temperature T_{BKT} determined by the superfluid density tensor. However, in traditional Zeeman field induced FFLO states, the effective superfluid density is extremely small (zero for Fulde-Ferrell (FF) states) due to the rotational symmetry of the Fermi surface, leading to extremely small T_{BKT} (zero for FF states) [17, 18]. Such small T_{BKT} holds even for 2D optical lattice systems, although there exists a large parameter region for the pseudogap phase with the FFLO type of order parameter (but no phase coherence and superfluidity) [11, 19]. This raises a realistic question whether FFLO states can indeed be observable in 2D at finite temperature.

In the past few years, synthetic spin-orbit (SO) coupling [20–26] has attracted increasing attention in cold atom community because of its key role in many intriguing physics such as topological superfluids [27–33], which can accommodate Majorana fermions in low dimensions with potential applications in fault-tolerant topological

quantum computation [34]. In SO coupled Fermi gases with an in-plane Zeeman field, FF superfluids are dominant in the low temperature phase diagram due to the asymmetric Fermi surface [35–42]. And with an additional out-of-plane Zeeman field, topological FF superfluids can emerge [43–50]. However, previous results are mainly based on mean-field theory, and one may wonder whether such FF superfluids can be observed experimentally at finite temperature in 2D through the BKT mechanism. Furthermore, these FF states exhibit gapless quasiparticle excitations in some parameter regions [36, 39, 47–50], and their stability may become a serious issue, similar as the well known unstable breached pair (BP) phases with *s*-wave contact interactions due to the divergence of fluctuations [51–53].

In this Letter, we address these crucial issues by studying 2D SO coupled Fermi gases with both in-plane and out-of-plane Zeeman fields in the presence of finite temperature phase fluctuations beyond mean-field theory. Our main findings are that: 1) The finite momenta of Cooper pairs lead to anisotropic superfluid densities along *x* and *y*. However, they are both nonzero and large, in contrast to zero transverse superfluid density in traditional Zeeman field induced FF superfluids. This leads to a finite BKT transition temperature, making it possible to observe FF superfluids in 2D. 2) The superfluid densities for gapless states are positive, implying that gapless FF superfluids are stable. 3) The changes of T_{BKT} with respect to Zeeman fields exhibit an inflection point, where the gap of the quasiparticle excitation spectrum at zero momentum closes. In particular, this inflectional behavior is stronger for a gapless state because of the higher density of states. 4) The anisotropic superfluid density tensor leads to anisotropic V-AV pairs below T_{BKT} .

Consider a 2D Rashba-type SO coupled Fermi gas with two equal-mass fermion species, labeled by up and down arrows respectively, subject to both in-plane (h_x) and out-of-plane (h_z) Zeeman fields and s -wave attractive contact interactions. The 2D system can be realized experimentally by a strong harmonic trap or deep optical lattices, which freeze atoms to the ground state along the third dimension. The many-body Hamiltonian reads

$$H = \int d\mathbf{r} \hat{\Psi}^\dagger(\mathbf{r}) H_s(\hat{\mathbf{p}}) \hat{\Psi}(\mathbf{r}) - U \int d\mathbf{r} \hat{\Psi}_\uparrow^\dagger(\mathbf{r}) \hat{\Psi}_\downarrow^\dagger(\mathbf{r}) \hat{\Psi}_\downarrow(\mathbf{r}) \hat{\Psi}_\uparrow(\mathbf{r}), \quad (1)$$

where the single particle Hamiltonian $H_s(\hat{\mathbf{p}}) = \frac{\hat{\mathbf{p}}^2}{2m} - \mu + H_{\text{SOC}}(\hat{\mathbf{p}}) + H_z$ with momentum operator $\hat{\mathbf{p}} = -i\hbar(\partial_x \mathbf{e}_x + \partial_y \mathbf{e}_y)$, chemical potential μ , attractive interaction strength U , and atom mass m . The Rashba SO coupling $H_{\text{SOC}}(\hat{\mathbf{p}}) = \alpha(\boldsymbol{\sigma} \times \hat{\mathbf{p}}) \cdot \mathbf{e}_z$ with Pauli matrices σ ; the Zeeman field $H_z = h_x \sigma_x + h_z \sigma_z$ along x and z . $\hat{\Psi}(\mathbf{r}) = [\hat{\Psi}_\uparrow(\mathbf{r}), \hat{\Psi}_\downarrow(\mathbf{r})]^T$ and $\hat{\Psi}_\nu^\dagger(\mathbf{r})$ ($\hat{\Psi}_\nu(\mathbf{r})$) creates (annihilates) a fermionic atom at \mathbf{r} .

In quantum field theory, the partition function at temperature $T = 1/\beta$ can be written as a path integral (See supplementary materials S-1) $Z = \int D(\bar{\Delta}, \Delta) e^{-S_{\text{eff}}[\bar{\Delta}, \Delta]}$ with the effective action written as $S_{\text{eff}}[\bar{\Delta}, \Delta] = \int_0^\beta d\tau \int d\mathbf{r} \frac{|\Delta|^2}{U} - \frac{1}{2} \ln \det G^{-1}$, where the inverse single particle Green function $G^{-1} = -\partial_\tau - H_B$ in the Nambu-Gor'kov basis, with 4×4 Bogoliubov-de Gennes (BdG) Hamiltonian

$$H_B = \begin{pmatrix} H_s(\hat{\mathbf{p}}) & \Delta(\mathbf{r}, \tau) \\ \Delta(\mathbf{r}, \tau) & -\sigma_y H_s(\hat{\mathbf{p}})^* \sigma_y \end{pmatrix}. \quad (2)$$

By assuming $\Delta(\mathbf{r}) = \Delta_0 e^{iQ_y y}$ given the Fermi surface asymmetry along y [42], the mean-field saddle point without phase fluctuations can be obtained by the saddle equations $\partial\Omega/\partial\Delta_0 = 0$, $\partial\Omega/\partial Q_y = 0$, and the particle number equation $\partial\Omega/\partial\mu = -n$ with a fixed total density n [47]. $\Omega = S_{\text{eff}}/\beta$ is the thermodynamical potential. Here the ultra-violet divergence can be regularized by $1/U = \sum_{\mathbf{k}} 1/(\hbar^2 k^2/m + E_b)$ with the binding energy E_b .

To study the effects of phase fluctuations, we set $\Delta(\mathbf{r}, \tau) = \Delta_0 e^{iQ_y y + i\theta(\mathbf{r}, \tau)}$, where $\theta(\mathbf{r}, \tau)$ is the phase fluctuations around the saddle point. Note that we have neglected the amplitude fluctuations corresponding to the gapped excitations. The inverse Green function $G^{-1} = G_0^{-1} + \Sigma$ with the mean-field one G_0^{-1} and self-energy $\Sigma = (i\partial_\tau\theta/2 + \hbar^2 Q_y \partial_y \theta/(4m) + \hbar^2 (\nabla\theta)^2/(8m))\sigma_z \otimes \sigma_0 + \hbar \nabla\theta \cdot \hat{\mathbf{p}}/(2m) - i\hbar^2 \nabla^2 \theta/(4m) + (\alpha \hbar \partial_x \theta/2)(\sigma_0 \otimes \sigma_y) - (\alpha \hbar \partial_y \theta/2)(\sigma_0 \otimes \sigma_x)$. The effective action $S_{\text{eff}} = S_{\text{eff}}^0 + S_{\text{eff}}^{\text{fluc}}$ with the contribution of the fluctuations $S_{\text{eff}}^{\text{fluc}} = \text{tr} \sum_{l=1}^\infty (G_0 \Sigma)^l/(2l)$. Expanding it to the second order yields

$$S_{\text{eff}}^{\text{fluc}} = \frac{1}{2} \int_0^\beta d\tau \int d\mathbf{r} [J_{xx}(\partial_x \theta)^2 + J_{yy}(\partial_y \theta)^2 + J_{\tau y} i \partial_\tau \theta \partial_y \theta + P(\partial_\tau \theta)^2 - i A \partial_\tau \theta], \quad (3)$$

with the superfluid density tensor $J_{\nu\mu}$ (here $J_{xy} = 0$), the corresponding superfluid density $\rho_{\mu\nu} = 4mJ_{\mu\nu}/(\hbar^2 n)$ scaled by the fixed total density, and the compressibility P . Compared with the formula for the normal superfluids [16], one additional term $J_{\tau y}$ emerges because of the nonzero Cooper pairing momenta Q_y . Note that these parameters cannot be expressed analytically and they are obtained via numerical approach (See supplementary materials S-1). We have checked that the results without h_x are exactly the same as previous ones [16].

By decomposing the phase $\theta(\mathbf{r}, \tau)$ into two parts: a static vortex configuration $\theta(\mathbf{r})_v$ and a time-dependent spin-wave one $\theta(\mathbf{r}, \tau)_{\text{sw}}$, the effective action contributed by phase fluctuations can be written as $S_{\text{eff}}^{\text{fluc}} = S_{\text{eff}}^v + S_{\text{eff}}^{\text{sw}}$, where the vortex part $S_{\text{eff}}^v = \frac{1}{2} \int d\mathbf{r} \sum_{\nu=x,y} J_{\nu\nu} (\partial_\nu \theta_v)^2$ and spin-wave part $S_{\text{eff}}^{\text{sw}} = \frac{1}{2} \int d\mathbf{r} [\sum_{\nu=x,y} J_{\nu\nu} (\partial_\nu \theta_{\text{sw}})^2 + J_{\tau y} i \partial_\tau \theta_{\text{sw}} + P(\partial_\tau \theta_{\text{sw}})^2 - i A \partial_\tau \theta_{\text{sw}}]$. The integration of the spin-wave part gives $S_{\text{eff}}^{\text{sw}} = \sum_{\mathbf{k}} \ln(1 - e^{-\beta E_{\text{sw}}(\mathbf{k})})$ where the spin-wave excitation $E_{\text{sw}}(\mathbf{k}) = \frac{1}{2P} [-J_{\tau y} k_y + \sqrt{J_{\tau y}^2 k_y^2 + 4P(J_{xx} k_x^2 + J_{yy} k_y^2)}]$. This anisotropic linear spectrum has anisotropic sound speeds: $v_x = \sqrt{J_{xx}/P}$ along x and $v_{y\pm} = \frac{1}{2P} (\mp J_{\tau y} + \sqrt{J_{\tau y}^2 + 4PJ_{yy}})$ along positive and negative y directions [47]. We note that the anisotropic sound speed also exists in other anisotropic superfluid systems [54], whereas the anisotropic behavior between the opposite directions among superfluids can occur only in FF superfluids. In normal BCS superfluids, $Q_y = 0$ and $v = \sqrt{J_{xx}/P}$ [14, 16].

With phase fluctuations, the parameters Δ_0 , Q_y , and μ can be calculated by self-consistently solving the saddle equations $\partial\Omega^0/\partial\Delta_0 = 0$, $\partial\Omega/\partial Q_y = 0$, and the particle number equation $\partial\Omega/\partial\mu = -n$, where $\Omega^0 = S_{\text{eff}}^0/\beta$ and $\Omega = S_{\text{eff}}/\beta$. Instead of the critical temperature determined by $\Delta_0 = 0$ in the mean-field theory, the critical BKT temperature is determined [13, 18, 54] (See supplementary materials S-2) by

$$T_{\text{BKT}} = \frac{\pi}{2} \sqrt{\prod_{\nu=x,y} J_{\nu\nu}(\Delta_0, Q_y, \mu, T_{\text{BKT}})}. \quad (4)$$

Note that J_{xx} and J_{yy} can be renormalized by the renormalization group theory, which does not change the physics qualitatively [55]. Across T_{BKT} that is much lower than the mean-field critical temperature, Fermi gases transit from a pseudogap phase (with nonzero Δ_0 but without phase coherence) to a superfluid affluent with V-AV pairs (with both pairing and phase coherence). We calculate T_{BKT} by solving the saddle point equations, the particle number equation, and Eq.(4) self-consistently. Here, the energy unit is chosen as the Fermi energy $E_F = \hbar^2 K_F^2/2m$ with Fermi vector $K_F = (2\pi n)^{1/2}$.

The BKT phase transition for FF states was studied for imbalanced Fermi gases without SO coupling and it was found that the superfluid density in the direction

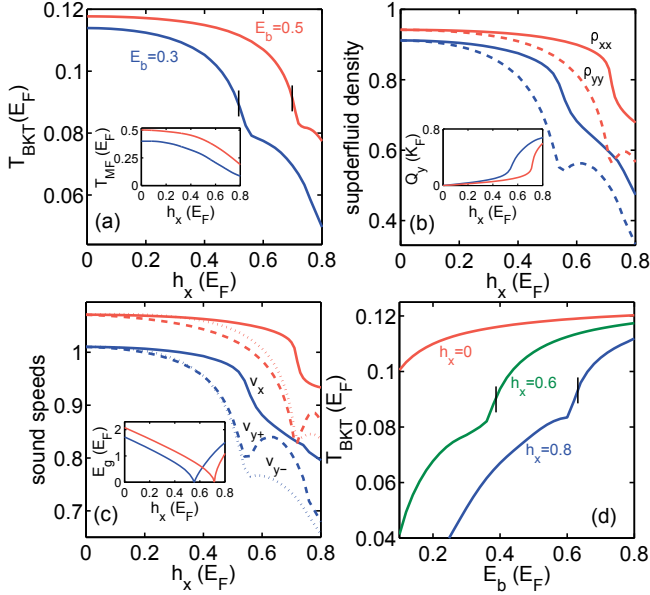


FIG. 1: (Color online) Plot of T_{BKT} (in (a)), superfluid densities and sound speeds (in (b) and (c)) evaluated at T_{BKT} , as a function of h_x with $E_b = 0.3E_F$ and $E_b = 0.5E_F$. The transition from gapped to gapless superfluids is marked by a short vertical line. In the inset of (a), (b), and (c), the mean-field critical temperatures, the momentum of Cooper pairs Q_y at T_{BKT} , and the gap at zero momentum at T_{BKT} are plotted respectively. The unit of the speed of sounds is $v_F/\sqrt{2}$ with Fermi velocity v_F and the unit of superfluid densities is n . In (b), the solid and dashed lines correspond to ρ_{xx} and ρ_{yy} respectively. In (c), the solid, dashed, and dotted lines respectively correspond to the sound speeds along the x direction v_x , positive y direction v_{y+} , and negative y direction v_{y-} . (d) Plot of T_{BKT} with respect to the binding energy E_b at fixed h_x . Here $\alpha K_F = E_F$ and $h_z = 0$.

perpendicular to the finite momenta of Cooper pairs is zero due to the rotational invariance of the Fermi surface [56], suggesting that FF superfluids may not be observable at finite temperature in 2D. Even considering the LO state, the critical temperature is still much lower because of the extremely high anisotropy of the superfluid density [17]. However, in Fig. 1, we find that the BKT critical temperature T_{BKT} for the FF superfluids is finite and large. Although the superfluid densities are still anisotropic with $\rho_{xx} > \rho_{yy}$ (shown in Fig. 1 (b)) due to the deformation of the equal thermodynamic potential along y , this anisotropy is not high enough to destroy the superfluidity at finite temperature in sharp contrast to $\rho_{yy} > \rho_{xx} = 0$ for traditional FF states without SO coupling [17, 18]. This result provides the theoretical foundation for the feasibility of observing FF states at finite temperature in 2D systems. Furthermore, T_{BKT} is much lower than mean-field transition temperature (shown in the inset of Fig. 1 (a)) as expected, whereas the finite momenta (shown in the inset of Fig. 1 (b)) evaluated at T_{BKT} of Cooper pairs are not destroyed by phase fluc-

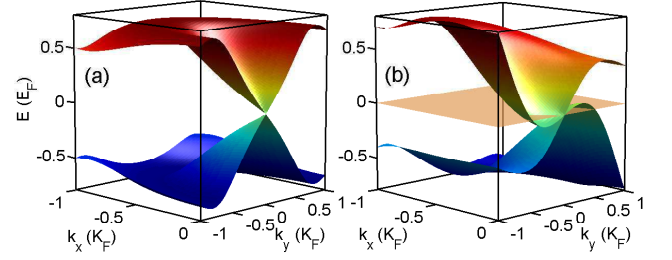


FIG. 2: (Color online) Quasiparticle excitations in the (k_x, k_y) plane at the critical point (a) from normal superfluids to topological superfluids, where $h_x = 0$ and $h_z = 0.652E_F$; and (b) from gapless FF superfluids to gapless topological FF superfluids, where $h_x = 0.5E_F$ and $h_z = 0.282E_F$. The physical quantities are evaluated at T_{BKT} . The light color plane in (b) corresponds to zero excitation energy. Here $\alpha K_F = E_F$ and $E_b = 0.3E_F$.

tuations.

With increasing h_x , the FF superfluids transit from gapped to gapless states [36, 39, 47–50] due to the strong distortion of quasiparticle excitations along y . The gapless FF superfluids exhibit a Fermi surface in quasiparticle spectrum as shown in Fig. 2(b). For a gapless superfluid, it is important to inquire whether they are stable. For instance, the famous gapless BP phase [51] with simple s -wave contact interactions was shown to be unstable with a negative superfluid density [52, 53]. In Fig. 1, we see that the superfluid densities for gapless states (the critical point of which is marked by a short line) are positive and T_{BKT} is finite, implying that the superfluids are stable. Furthermore, there is an inflection point near the gapless transition point, corresponding to the minimum of the superfluid density and sound speeds. This point is exactly where the gap at zero momentum of quasiparticle excitations (shown in the inset of Fig. 1(c)) closes as $\bar{h}_x^2 = \bar{\mu}^2 + \Delta_0^2$ with $\bar{h}_x = h_x + \alpha Q_y/2$ and $\bar{\mu} = \mu - Q_y^2/8m$, suggesting that phase fluctuations have dramatic effects at zero momentum (long wavelength limit), whereas the gapless surface emerges at nonzero momenta. Analogous to the anisotropic superfluid density tensor, the sound speeds shown in Fig. 1(c) are anisotropic along the x and y directions and even different along the positive and negative y directions, which is unique for FF superfluids. The anisotropy increases with the increasing of Q_y with respect to h_x until the speed of sounds reaches the minimum where the gap at zero momentum closes. At $h_x = 0$, $v_x = v_{y+} = v_{y-}$ with the value close to $v_F/\sqrt{2}$ in the BCS limit.

In Fig. 1 (d), we plot the BKT temperature with respect to the binding energy E_b at fixed Zeeman fields. T_{BKT} is a monotonically increasing function of E_b , and approaches a constant value at large E_b that is independent of h_x , signaling the crossover from BCS Cooper pairs to Bose-Einstein condensates of tightly bound molecules. Also, the increased Δ_0 by increasing E_b closes the gap at

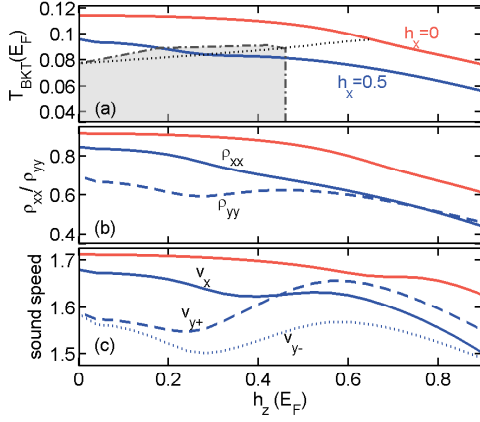


FIG. 3: (Color online) Plot of T_{BKT} (in (a)), superfluid density (in (b)) and sound speeds (in (c)) evaluated at T_{BKT} , as a function of h_z with h_x fixed. The states are FF superfluids except the one with $h_x = 0$. The black dotted line connects the topological transition points as h_x varies. The grey area surrounded by the dashed-dotted line maps out the gapless state region. The red and blue lines correspond to $h_x = 0, 0.5E_F$ respectively in all figures. Here $\alpha K_F = E_F$ and $E_b = 0.3E_F$.

zero momentum when $\bar{h}_x^2 = \bar{\mu}^2 + \Delta_0^2$, where there emerges an inflection point accompanied by the critical transition point between gapless and gapped FF superfluids. Without Zeeman fields ($h_x = 0$), no gap closing point at zero momentum appears and thus no inflection point.

To demonstrate the effects of h_z Zeeman field, we plot the change of the BKT temperature T_{BKT} ((a)), the superfluid density ((b)), and the speeds of sound ((c)) with respect to h_z for fixed h_x in Fig. S1. Clearly, T_{BKT} is a monotonically decreasing function of Zeeman fields since both Zeeman fields are detrimental to the Cooper pairing. Superfluid density and sound speeds are both anisotropic similar to the pure h_x scenario. On the other hand, given that the quasiparticle gap at zero momentum first closes and then reopens at the topological transition point [43–50] $h_z^2 = \bar{\mu}^2 + \Delta_0^2 - \bar{h}_x^2$ driven by h_z field, one may expect an inflectional or minimum behavior at this point, similar to the case with pure h_x field. Indeed, there is a manifest inflection point for T_{BKT} and minimum points for superfluid density and sound speeds in gapless topological superfluids (e.g. blue line in Fig. S1). However, this inflectional or minimum behavior is much smaller in either topological superfluids or topological FF superfluids with zero or small h_x (e.g. red line in Fig. S1. See also supplementary materials S-3) because of the lower density of states at zero momentum compared with that in gapless topological superfluids as visualized in Fig. 2.

In Fig. S1(a), the dotted line represents T_{BKT} at the topological transition points as h_x varies, showing that T_{BKT} decreases with increasing h_x while the critical h_z decreases [43]. This indicates that the existence of h_x cannot enhance the BKT temperature for the observa-

tion of topological superfluids. The grey region [57] surrounded by the dashed-dotted line is where the gapless superfluids can be observed. Compared with the 3D case where the gapless superfluids (including both topological and topological trivial phases) are dominant [47], this gapless region is much smaller because the gap at $\mathbf{k} = 0$ reopens across the topological transition point.

Below the BKT temperature, the superfluids are affluent with V-AV pairs, which can be obtained by solving $\nabla \times \mathbf{v}_s = 2\pi \sum_i n_i \delta(\mathbf{r} - \mathbf{r}_i)$ and the minimization of S_{eff}^v : $\rho_{xx} \partial_x^2 \theta_v + \rho_{yy} \partial_y^2 \theta_v = 0$. Here $\mathbf{v}_s = \nabla \theta_v(\mathbf{r})$, $n_i = \pm 1$ represents a vortex or antivortex localized at \mathbf{r}_i . For a single vortex, $\theta_v = \arctan(\rho^2 y/x)$ with $\rho = (\rho_{xx}/\rho_{yy})^{1/4}$. For a V-AV pair located at $(\pm x_0, 0)$, $\theta_v = \arctan[2\bar{x}_0\bar{y}/(\bar{x}_0^2 - \bar{x}^2 - \bar{y}^2)]$ with $\bar{x} = x/\rho, \bar{y} = y/\rho$, and $\bar{a} = a/\rho$. Interestingly, the anisotropic superfluid densities induced by the finite momentum pairing results in anisotropic V-AV pairs (See supplementary materials S-4) in contrast to isotropic ones in normal BCS superfluids for Rashba-type SO coupled Fermi gases [14–16, 58]. Anisotropic V-AV pairs have also been discussed recently where the anisotropy is caused by the anisotropic SO coupling [54], instead of FF pairing here.

For Fermi gases, the pseudogap phenomenon beyond the BKT temperature has been observed in 2D ^{40}K fermionic atoms with the number of atoms on the order of 10^3 and the harmonic trap frequency $2\pi \times 127\text{Hz}$ [59]. Equal Rashba and Dresselhaus (ERD) SO coupling as well as Zeeman fields have also been engineered in these atom gases [21, 22] by coupling two hyperfine states using Raman lasers [20–26]. The experimental realization of Rashba SO coupling is currently under investigation. The large BKT temperature conclusion should also apply to the FF states in the ERD-type SO coupled Fermi superfluids because of the same mechanism for inducing FF type Cooper pairs [36, 42]. Recently, the observation of quasi long-range order in 2D ^6Li gases has been reported [60] and the number of atoms can be as large as 5×10^4 . Similar experimental setup may be employed to realize the FF superfluids in 2D with the feature: anisotropic sound speeds, which can be experimentally probed through the density perturbation [61]. Also other methods, such as observing the anisotropic V-AV pairs by time-of-flight expansion or Bragg scattering can be considered. We note that in real experiments the BKT transition occurs as the BKT crossover because of finite-size effects as shown in the 2D BEC experiment [62].

In summary, we investigate the BKT phase transition in a 2D SO coupled Fermi gas subject to Zeeman fields and find finite BKT temperatures for both gapped and gapless FF superfluids in sharp contrast to the case without SO coupling, where it is zero due to the vanishing transverse superfluid density. Our findings demonstrate the feasibility for the experimental observation of FF superfluids (gapped or gapless, topological or non-topological) and the associated topological excitations

(e.g., Majorana fermions) in a 2D SO coupled Fermi gas at finite temperature.

Acknowledgements: This work is supported by ARO (W911NF-12-1-0334) and AFOSR (FA9550-11-1-0313 and FA9550-13-1-0045). We thank Texas Advanced Computing Center (TACC), where our numerical simulations were performed.

-
- * Corresponding Author, Email: chuanwei.zhang@utdallas.edu
- [1] P. Fulde and R. A. Ferrell, *Phys. Rev.* **135**, A550 (1964).
 - [2] A. I. Larkin and Yu. N. Ovchinnikov, *Zh. Eksp. Teor. Fiz.* **47**, 1136 (1964) [*Sov. Phys. JETP* **20**, 762 (1965)].
 - [3] H. A. Radovan, N. A. Fortune, T. P. Murphy, S. T. Hannahs, E. C. Palm, S. W. Tozer, and D. Hall, *Nature* **425**, 51 (2003).
 - [4] A. Bianchi, R. Movshovich, C. Capan, P. G. Pagliuso, and J. L. Sarrao, *Phys. Rev. Lett.* **91**, 187004 (2003).
 - [5] M. Kenzelmann, Th. Strässle, C. Niedermayer, M. Sigrist, B. Padmanabhan, M. Zolliker, A. D. Bianchi, R. Movshovich, E. D. Bauer, J. L. Sarrao, and J. D. Thompson, *Science* **321** 1652 (2008).
 - [6] S. Uji, T. Terashima, M. Nishimura, Y. Takahide, T. Konoike, K. Enomoto, H. Cui, H. Kobayashi, A. Kobayashi, H. Tanaka, M. Tokumoto, E. S. Choi, T. Tokumoto, D. Graf, and J. S. Brooks, *Phys. Rev. Lett.* **97**, 157001 (2006).
 - [7] L. Li, C. Richter, J. Mannhart, and R. C. Ashoori, *Nature* **7**, 762 (2011).
 - [8] Y. Liao, A. S. C. Rittner, T. Paprotta, W. Li, G. B. Partridge, R. G. Hulet, S. K. Baur, and E. J. Mueller, *Nature* **467**, 567 (2010).
 - [9] D. E. Sheehy and L. Radzihovsky, *Phys. Rev. Lett.* **96**, 060401 (2006).
 - [10] M. M. Parish, S. K. Baur, E. J. Mueller, and D. A. Huse, *Phys. Rev. Lett.* **99**, 250403 (2007).
 - [11] T. K. Koponen, T. Paananen, J.-P. Martikainen, M. R. Bakhtiari, P. Törmä, *New Journal of Physics* **10**, 045014 (2008).
 - [12] V. L. Berezinskii, *Sov. Phys. JETP* **32**, 493 (1971).
 - [13] J. M. Kosterlitz and D. Thouless, *J. Phys. C* **5**, L124 (1972); **6**, 1181 (1973).
 - [14] S. S. Botelho and C. A. R. Sá de Melo, *Phys. Rev. Lett.* **96**, 040404 (2006).
 - [15] L. He and X. -G. Huang, *Phys. Rev. Lett.* **108**, 145302 (2012).
 - [16] M. Gong, G. Chen, S. Jia, and C. Zhang, *Phys. Rev. Lett.* **109**, 105302 (2012).
 - [17] L. Radzihovsky and A. Vishwanath, *Phys. Rev. Lett.* **103**, 010404 (2009).
 - [18] S. Yin, J. -P. Martikainen, and P. Törmä, *Phys. Rev. B* **89**, 014507 (2014).
 - [19] M. J. Wolak, B. Grémaud, R. T. Scalettar, and G. G. Batrouni, *Phys. Rev. A* **86**, 023630 (2012).
 - [20] Y. -J. Lin, K. Jiménez-García, and I. B. Spielman, *Nature (London)* **471**, 83 (2011).
 - [21] P. Wang, Z. -Q. Yu, Z. Fu, J. Miao, L. Huang, S. Chai, H. Zhai, and J. Zhang, *Phys. Rev. Lett.* **109**, 095301 (2012).
 - [22] L. W. Cheuk, A. T. Sommer, Z. Hadzibabic, T. Yefsah, W. S. Bakr, and M. W. Zwierlein, *Phys. Rev. Lett.* **109**, 095302 (2012).
 - [23] J. -Y. Zhang, S. -C. Ji, Z. Chen, L. Zhang, Z. -D. Du, B. Yan, G. -S. Pan, B. Zhao, Y. -J. Deng, H. Zhai, S. Chen, and J. -W. Pan, *Phys. Rev. Lett.* **109**, 115301 (2012).
 - [24] C. Qu, C. Hamner, M. Gong, C. Zhang, and P. Engels, *Phys. Rev. A* **88**, 021604(R) (2013).
 - [25] R. A. Williams, M. C. Beeler, L. J. LeBlanc, K. Jiménez-García, and I. B. Spielman, *Phys. Rev. Lett.* **111**, 095301 (2013).
 - [26] V. Galitski and I. B. Spielman, *Nature (London)* **494**, 49 (2013).
 - [27] C. Zhang, S. Tewari, R. M. Lutchyn, and S. Das Sarma, *Phys. Rev. Lett.* **101**, 160401 (2008).
 - [28] M. Sato, Y. Takahashi, and S. Fujimoto, *Phys. Rev. Lett.* **103**, 020401 (2009).
 - [29] S. -L. Zhu, L. -B. Shao, Z. D. Wang, and L. -M. Duan, *Phys. Rev. Lett.* **106**, 100404 (2011).
 - [30] L. Jiang, T. Kitagawa, J. Alicea, A. R. Akhmerov, D. Pekker, G. Refael, J. I. Cirac, E. Demler, M. D. Lukin, and P. Zoller, *Phys. Rev. Lett.* **106**, 220402 (2011).
 - [31] L.-J. Lang, X. Cai, and S. Chen, *Phys. Rev. Lett.* **108**, 220401 (2012).
 - [32] X. Zhou, Y. Li, Z. Cai, and C. Wu, *J. Phys. B: At. Mol. Opt. Phys.* **46**, 134001 (2013).
 - [33] X. -J. Liu, K. T. Law, and T. K. Ng, *Phys. Rev. Lett.* **112**, 086401 (2014).
 - [34] A. Kitaev, *Ann. Phys. (N. Y.)* **303**, 2 (2003).
 - [35] Z. Zheng, M. Gong, X. Zou, C. Zhang, and G. Guo, *Phys. Rev. A* **87**, 031602(R) (2013).
 - [36] F. Wu, G.-C. Guo, W. Zhang, and W. Yi, *Phys. Rev. Lett.* **110**, 110401 (2013).
 - [37] X.-J. Liu and H. Hu, *Phys. Rev. A* **87**, 051608(R) (2013).
 - [38] Z. Fu, L. Huang, Z. Meng, P. Wang, X.-J. Liu, H. Pu, H. Hu, and J. Zhang, *Phys. Rev. A* **87**, 053619 (2013).
 - [39] L. Dong, L. Jiang, and H. Pu, *New Journal of Physics* **15**, 075014 (2013).
 - [40] H. Hui and X.-J. Liu, *New Journal of Physics* **15**, 093037 (2013).
 - [41] M. Iskin, *Phys. Rev. A* **88**, 013631 (2013).
 - [42] Y. Xu, C. Qu, M. Gong, and C. Zhang, *Phys. Rev. A* **89**, 013607 (2014).
 - [43] C. Qu, Z. Zheng, M. Gong, Y. Xu, L. Mao, X. Zou, G. Guo, and C. Zhang, *Nature Communications* **4**, 2710 (2013).
 - [44] W. Zhang and W. Yi, *Nature Communications* **4**, 2711 (2013).
 - [45] X. -J. Liu and H. Hu, *Phys. Rev. A* **88**, 023622 (2013).
 - [46] C. Chen, *Phys. Rev. Lett.* **111**, 235302 (2013).
 - [47] Y. Xu, R.-L. Chu, and C. Zhang, *Phys. Rev. Lett.* **112**, 136402 (2014).
 - [48] C. F. Chan and M. Gong, *Phys. Rev. B* **89**, 174501 (2014).
 - [49] Y. Cao, S.-H. Zou, X.-J. Liu, S. Yi, G.-L. Long, and H. Hu, *arXiv:1402.6832*.
 - [50] H. Hu, L. Dong, Y. Cao, H. Pu, and X. -J. Liu, *arXiv:1404.2442*.
 - [51] W. V. Liu and F. Wilczek, *Phys. Rev. Lett.* **90**, 047002 (2003).
 - [52] S.-T. Wu and S. Yip, *Phys. Rev. A* **67**, 053603 (2003).
 - [53] M. M. Forbes, E. Gubankova, W. V. Liu, and F. Wilczek, *Phys. Rev. Lett.* **94**, 017001 (2005).
 - [54] J. P. A. Devreese, J. Tempere, and C. A. R. Sá de Melo,

- Phys. Rev. Lett. **113**, 165304 (2014).
- [55] H. T. C. Stoof, K. B. Gubbels, and D. B. M. Dickerscheid, *Ultracold Quantum Fields* (Springer, Dordrecht, 2009).
- [56] The thermodynamical potential is degenerate for the center-of-mass \mathbf{Q} along a ring, i.e. $\Omega = \Omega(|\mathbf{Q}|)$ for the traditional Zeeman field induced FF superfluids. Such degeneracy leads to zero transverse superfluid density. See also Ref. [17, 18].
- [57] The grey region corresponds to the area $T < T_{BKT}(h_x, h_z)$, where the excitation gap (i.e. the minimum of the particle branch) $E_g < 0$.
- [58] K. Zhou and Z. Zhang, Phys. Rev. Lett. **108**, 025301 (2012).
- [59] M. Feld, B. Fröhlich, E. Vogt, M. Koschorreck, and M. Köhl, Nature **480**, 75 (2011).
- [60] M. G. Ries, A. N. Wenz, G. Zürn, L. Bayha, I. Boettcher, D. Kedar, P. A. Murthy, M. Neidig, T. Lompe, and S. Jochim, arXiv:1409.5373.
- [61] M. R. Andrews, D. M. Kurn, H.-J. Miesner, D. S. Durfee, C. G. Townsend, S. Inouye, and W. Ketterle, Phys. Rev. Lett. **79**, 553 (1997); J. Joseph, B. Clancy, L. Luo, J. Kinast, A. Turlapov, and J. E. Thomas, Phys. Rev. Lett. **98**, 170401 (2007).
- [62] Z. Hadzibabic, P. Krüger, M. Cheneau, B. Battelier, and J. Dalibard, Nature **441**, 1118 (2006).

In the main text we present various physical quantities including the BKT temperature, superfluid density tensor, and speed of sound for a spin-orbit coupled Fermi gas subject to both in-plane and out-of-plane Zeeman fields. Here we provide more detailed calculation information in Sec. S-1 and S-2, plot the BKT temperature, superfluid density, and sound speeds for more parameters in Sec. S-3, and also plot anisotropic V-AV pair structures in Sec. S-4.

S-1. DERIVATION OF SUPERFLUID DENSITY TENSOR AND SOUND SPEED

In quantum field theory, the partition function can be written as $Z = \text{Tr}(e^{-\beta H}) = \int D(\bar{\psi}, \psi) e^{-S_{\text{eff}}[\bar{\psi}, \psi]}$ with $\beta = 1/T$ at the temperature T . The effective action is

$$S_{\text{eff}}[\bar{\psi}, \psi] = \int_0^\beta d\tau \left(\int d\mathbf{r} \sum_\sigma \bar{\psi}_\sigma(\mathbf{r}, \tau) \partial_\tau \psi_\sigma(\mathbf{r}, \tau) + H(\bar{\psi}, \psi) \right), \quad (\text{S1})$$

where $\int d\tau$ is an integral over the imaginary time τ and $H(\bar{\psi}, \psi)$ is obtained by replacing $\hat{\Psi}_\sigma^\dagger$ and $\hat{\Psi}_\sigma$ with Grassman field number $\bar{\psi}_\sigma$ and ψ_σ . We can transform the quartic interaction term to quadratic one by Hubbard-Stratonovich transformation, where the order parameter $\Delta(\mathbf{r}, \tau)$ is defined. By integrating out fermion fields, the partition function becomes $Z = \int D(\bar{\Delta}, \Delta) e^{-S_{\text{eff}}[\bar{\Delta}, \Delta]}$, where the effective action can be written as

$$S_{\text{eff}}[\bar{\Delta}, \Delta] = \int_0^\beta d\tau \int d\mathbf{r} \left(\frac{|\Delta|^2}{U} \right) - \frac{1}{2} \ln \det G^{-1}. \quad (\text{S2})$$

Here the inverse single particle Green function $G^{-1} = -\partial_\tau - H_B$ in the Nambu-Gor'kov representation with 4×4 Bogoliubov-de Gennes (BdG) Hamiltonian (Eq.(2) in the main text)

$$H_B = \begin{pmatrix} H_s(\hat{\mathbf{p}}) & \Delta(\mathbf{r}, \tau) \\ \Delta(\mathbf{r}, \tau) & -\sigma_y H_s(\hat{\mathbf{p}})^* \sigma_y \end{pmatrix}. \quad (\text{S3})$$

Assume that a mean-field solution has the FF form $\Delta(\mathbf{r}, \tau)_0 = e^{iQ_y y} \Delta_0$ with the space independent Δ_0 given that the in-plane Zeeman field deforms the Fermi surface along the y direction, leading to finite momentum pairing along that direction [S1]. Through Fourier transformation and the summation of Matsubara frequency, this form of $\Delta(\mathbf{r}, \tau)$ yields mean-field thermodynamical potential [S2, S3].

To study the effects of phase fluctuations, we assume $\Delta(\mathbf{r}) = \Delta_0 e^{iQ_y y + i\theta(\mathbf{r})}$ with phase fluctuation field $\theta(\mathbf{r})$ around the saddle point. The unitary transformed inverse Green function becomes

$$G^{-1} = G_0^{-1} + \Sigma, \quad (\text{S4})$$

via the unitary operator

$$U = \begin{pmatrix} e^{i(\theta + Q_y y)} & 0 \\ 0 & e^{-i(\theta + Q_y y)} \end{pmatrix}. \quad (\text{S5})$$

Here G_0^{-1} represents the mean-field part and

$$\begin{aligned} \Sigma = & [i\partial_\tau \theta / 2 + \hbar^2 Q_y \partial_y \theta / (4m) + \hbar^2 (\nabla \theta)^2 / (8m)] \sigma_z \otimes \sigma_0 + \hbar \nabla \theta \cdot \hat{\mathbf{p}} / (2m) \\ & - i \hbar^2 \nabla^2 \theta / (4m) + (\alpha \hbar \partial_x \theta / 2) (\sigma_0 \otimes \sigma_y) - (\alpha \hbar \partial_y \theta / 2) (\sigma_0 \otimes \sigma_x), \end{aligned} \quad (\text{S6})$$

is the self-energy contributed by phase fluctuations. Substituting Eq. S4 to Eq. S2 leads to the effective action

$$S_{\text{eff}} = S_{\text{eff}}^0 + S_{\text{eff}}^{\text{fluc}}, \quad (\text{S7})$$

where $S_{\text{eff}}^{\text{fluc}} = \text{tr} \sum_{l=1}^{\infty} (G_0 \Sigma)^l / (2l)$ represents phase fluctuation contributions. Expanding it to the second order yields (Eq.(3) in the main text)

$$\begin{aligned} S_{\text{eff}}^{\text{fluc}} &= \frac{1}{2} \text{tr} G_0 \Sigma + \frac{1}{4} \text{tr} (G_0 \Sigma G_0 \Sigma) \\ &= \frac{1}{2} \int d\mathbf{r} \int d\tau [J_{xx}(\partial_x \theta)^2 + J_{yy}(\partial_y \theta)^2 + J_{xy} \partial_x \theta \partial_y \theta + iJ_{\tau y} \partial_\tau \theta \partial_y \theta + iJ_{\tau x} \partial_\tau \theta \partial_x \theta + P(\partial_\tau \theta)^2 - iA \partial_\tau \theta], \end{aligned} \quad (\text{S8})$$

where

$$J_{xx} = \frac{\hbar^2}{4m} n + \frac{1}{8\beta(2\pi)^2} \int d\mathbf{k} \sum_{\omega_n} \left(\hbar^2 \alpha^2 f_{44} + \frac{\hbar^2}{m^2} f_{22} k_x^2 + \frac{2\hbar^2 \alpha}{m} f_{24} k_x \right), \quad (\text{S9})$$

$$J_{yy} = \frac{\hbar^2}{4m} n + \frac{1}{8\beta(2\pi)^2} \int d\mathbf{k} \sum_{\omega_n} \left(\frac{\hbar^4}{4m^2} f_{11} Q_y^2 - \frac{\hbar^3 \alpha}{m} f_{15} Q_y + \hbar^2 \alpha^2 f_{55} + \frac{\hbar^3}{m^2} f_{12} Q_y k_y + \frac{\hbar^2}{m^2} f_{22} k_y^2 - \frac{2\hbar^2 \alpha}{m} f_{25} k_y \right), \quad (\text{S10})$$

$$J_{xy} = \frac{1}{4\beta(2\pi)^2} \int d\mathbf{k} \sum_{\omega_n} \left(\frac{\hbar^3 \alpha}{2m} f_{14} Q_y - \hbar^2 \alpha^2 f_{45} + \frac{\hbar^3}{2m^2} f_{12} Q_y k_x + \frac{\hbar^2}{m^2} f_{22} k_x k_y + \frac{\hbar^2 \alpha}{m} f_{24} k_y - \frac{\hbar^2 \alpha}{m} f_{25} k_x \right), \quad (\text{S11})$$

$$J_{\tau y} = \frac{1}{8\beta(2\pi)^2} \int d\mathbf{k} \sum_{\omega_n} \left(\frac{\hbar^2}{m} f_{11} Q_y - 2\hbar \alpha f_{15} + \frac{2\hbar}{m} f_{12} k_y \right), \quad (\text{S12})$$

$$J_{\tau x} = \frac{1}{4\beta(2\pi)^2} \int d\mathbf{k} \sum_{\omega_n} \left(\hbar \alpha f_{14} + \frac{\hbar}{m} f_{12} k_x \right), \quad (\text{S13})$$

$$P = -\frac{1}{8} \frac{1}{\beta(2\pi)^2} \int d\mathbf{k} \sum_{\omega_n} f_{11}, \quad (\text{S14})$$

$$A = n, \quad (\text{S15})$$

and

$$f_{11} = \text{tr}_4 G_0(-i\omega_n, \mathbf{k}) \sigma_z \otimes \sigma_0 G_0(-i\omega_n, \mathbf{k}) \sigma_z \otimes \sigma_0, \quad (\text{S16})$$

$$f_{12} = \text{tr}_4 G_0(-i\omega_n, \mathbf{k}) G_0(-i\omega_n, \mathbf{k}) \sigma_z \otimes \sigma_0, \quad (\text{S17})$$

$$f_{14} = \text{tr}_4 G_0(-i\omega_n, \mathbf{k}) \sigma_0 \otimes \sigma_y G_0(-i\omega_n, \mathbf{k}) \sigma_z \otimes \sigma_0, \quad (\text{S18})$$

$$f_{15} = \text{tr}_4 G_0(-i\omega_n, \mathbf{k}) \sigma_0 \otimes \sigma_x G_0(-i\omega_n, \mathbf{k}) \sigma_z \otimes \sigma_0, \quad (\text{S19})$$

$$f_{22} = \text{tr}_4 G_0(-i\omega_n, \mathbf{k}) G_0(-i\omega_n, \mathbf{k}), \quad (\text{S20})$$

$$f_{24} = \text{tr}_4 G_0(-i\omega_n, \mathbf{k}) \sigma_0 \otimes \sigma_y G_0(-i\omega_n, \mathbf{k}), \quad (\text{S21})$$

$$f_{25} = \text{tr}_4 G_0(-i\omega_n, \mathbf{k}) \sigma_0 \otimes \sigma_x G_0(-i\omega_n, \mathbf{k}), \quad (\text{S22})$$

$$f_{44} = \text{tr}_4 G_0(-i\omega_n, \mathbf{k}) \sigma_0 \otimes \sigma_y G_0(-i\omega_n, \mathbf{k}) \sigma_0 \otimes \sigma_y, \quad (\text{S23})$$

$$f_{45} = \text{tr}_4 G_0(-i\omega_n, \mathbf{k}) \sigma_0 \otimes \sigma_x G_0(-i\omega_n, \mathbf{k}) \sigma_0 \otimes \sigma_y, \quad (\text{S24})$$

$$f_{55} = \text{tr}_4 G_0(-i\omega_n, \mathbf{k}) \sigma_0 \otimes \sigma_x G_0(-i\omega_n, \mathbf{k}) \sigma_0 \otimes \sigma_x. \quad (\text{S25})$$

Here $G_0(-i\omega_n, \mathbf{k})$ is the Fourier transformation of $G_0(\mathbf{r}, \tau)$ with Matsubara frequency $\omega_n = (2n+1)\pi/\beta$; tr_4 represents the trace calculation for a 4×4 matrix. Note that we calculate the summation over Matsubara frequency numerically due to the absence of the analytical expression of G_0 .

Our numerical results show that $J_{xy} = 0$ and $J_{\tau x} = 0$ while $J_{\tau y} \neq 0$ for FF superfluids, which is reasonable considering that the symmetry of the quasi-particle excitations along the y direction is broken while that along the x

direction is kept. In the absence of Zeeman fields, these parameters can be analytically written as

$$\begin{aligned} J_{xx} &= J_{yy} \\ &= \frac{\hbar^2}{4m} \left[n - \frac{1}{(2\pi)^2} \int d\mathbf{k} \sum_{L=\pm} \left(\frac{\alpha^2 m}{4EL} \tanh(\beta E_L/2) \left(1 + L \frac{\epsilon_{\mathbf{k}}^2}{|\alpha|k|\xi_{\mathbf{k}}|} \right) + \frac{\beta m}{8\hbar^2} \left(\alpha - L \frac{\hbar \xi_{\mathbf{k}} k}{m|\xi_{\mathbf{k}}|} \right)^2 \text{sech}(\beta E_L/2)^2 \right) \right], \end{aligned} \quad (\text{S26})$$

$$P = \frac{1}{8(2\pi)^2} \int d\mathbf{k} \sum_{L=\pm} \left[\frac{\beta}{2} \text{sech}(\beta E_L/2)^2 \left(\frac{\xi_{\mathbf{k}}}{E_L} \right)^2 \left(1 + L \frac{|\alpha|k}{|\xi_{\mathbf{k}}|} \right)^2 + \frac{1}{E_L} \tanh(\beta E_L/2) \left(\frac{\Delta_0}{E_L} \right)^2 \right], \quad (\text{S27})$$

$$Q = n, \quad (\text{S28})$$

and $J_{xy} = J_{\tau y} = J_{\tau x} = 0$. Here the quasi-particle excitation spectrum is

$$E_L = \epsilon_{\mathbf{k}}^2 + \alpha^2 k^2 + 2Lk|\alpha\xi_{\mathbf{k}}|, \quad (\text{S29})$$

with $\xi_{\mathbf{k}} = \hbar^2 k^2/2m - \mu$ and $\epsilon_{\mathbf{k}} = \sqrt{\xi(\mathbf{k})^2 + \Delta_0^2}$. These expressions are exactly the same as previous results [S4]. For the FF superfluids, $Q_y \neq 0$, leading to $J_{xx} \neq J_{yy}$ corresponding to anisotropic superfluid densities.

To obtain the low energy excitation spectrum, we write the effective action in Fourier space

$$S_{\text{eff}}^{\text{fluc}} = \frac{1}{2} \sum_{\mathbf{k}n} (J_{xx}k_x^2 + J_{yy}k_y^2 - J_{\tau y}E_{\text{sw}}(\mathbf{k})k_y - PE_{\text{sw}}(\mathbf{k})^2) \theta(n, \mathbf{k})\theta(-n, -\mathbf{k}), \quad (\text{S30})$$

where $\theta(n, \mathbf{k})$ is the Fourier transformation of $\theta(\mathbf{r}, \tau)$; $i\omega_n$ has been taken analytically to $E_{\text{sw}}(\mathbf{k} + i0^+)$. The low energy excitation spectrum can be obtained by

$$PE_{\text{sw}}(\mathbf{k})^2 + J_{\tau y}k_y E_{\text{sw}}(\mathbf{k}) - J_{xx}k_x^2 - J_{yy}k_y^2 = 0, \quad (\text{S31})$$

which leads to the dispersion

$$E_{\text{sw}}(\mathbf{k}) = \frac{-J_{\tau y}k_y + \sqrt{J_{\tau y}^2 k_y^2 + 4P(J_{xx}k_x^2 + J_{yy}k_y^2)}}{2P}. \quad (\text{S32})$$

Clearly, the dispersion along each direction is linear around $k = 0$, with the slope (i.e. sound speeds) written as

$$v_x = \sqrt{\frac{J_{xx}}{P}}, \quad (\text{S33})$$

$$v_{y+} = \frac{-J_{\tau y} + \sqrt{J_{\tau y}^2 + 4PJ_{yy}}}{2P}, \quad (\text{S34})$$

$$v_{y-} = \frac{J_{\tau y} + \sqrt{J_{\tau y}^2 + 4PJ_{yy}}}{2P}. \quad (\text{S35})$$

In normal superfluids where $J_{\tau y} = 0$ and $J_{xx} = J_{yy}$, the speeds of sound are isotropic. However, in FF superfluids where $J_{\tau y} \neq 0$ and $J_{xx} \neq J_{yy}$, they are anisotropic and even different along the positive and negative y directions. It is important to note that anisotropic sound speeds also happen in anisotropic systems such as equal Rashba-Dresselhaus spin-orbit coupled Fermi gases [S5] where $J_{xx} \neq J_{yy}$, but in that system $J_{\tau y} = 0$, implying that they are the same along the positive and negative y directions.

The integration of spin-wave part yields

$$S_{\text{eff}}^{\text{sw}} = \sum_{\mathbf{k}} \ln \left(1 - e^{-\beta E_{\text{sw}}(\mathbf{k})} \right). \quad (\text{S36})$$

In the presence of spin-wave excitations, the generalized saddle point equation and particle number equation become $\partial\Omega^0/\partial\Delta_0 = 0$, $\partial\Omega/\partial Q_y = 0$, and $\partial\Omega/\partial\mu = -n$.

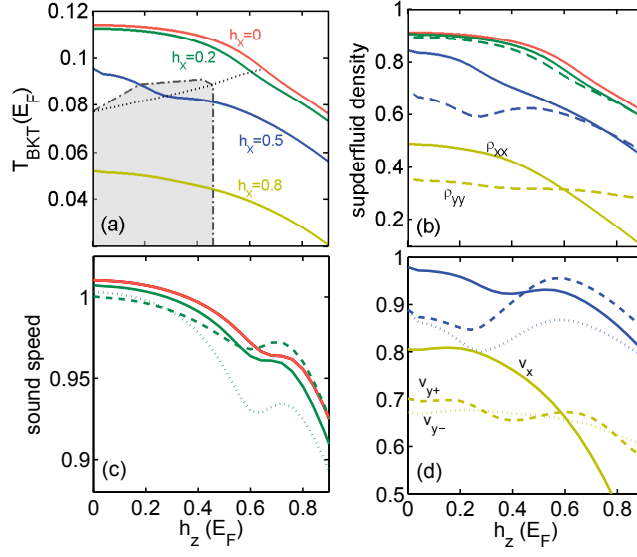


FIG. S1: (Color online) Plot of T_{BKT} (in (a)), superfluid density (in (b)) and sound speeds (in (c) and (d)) evaluated at T_{BKT} , as a function of h_z with h_x fixed. All states are FF superfluids except the one with $h_x = 0$. The black dotted line connects the topological transition points as h_x varies. The grey area surrounded by the dashed-dotted line maps out the gapless states region. In (b) the solid and dashed lines label the superfluid densities along x and y directions respectively and in (c) and (d) the solid, dashed and dotted lines label the sound speeds along x , positive y , and negative y directions respectively. The red, green, blue, and yellow lines correspond to $h_x = 0, 0.2E_F, 0.5E_F, 0.8E_F$ respectively in all figures. Here $\alpha K_F = E_F$ and $E_b = 0.3E_F$.

S-2. GENERALIZED KOSTERLITZ-THOULESS RELATION

For FF superfluids with anisotropic superfluid densities, the KT relation [S6, S7] corresponding to isotropic superfluid densities should be generalized. We consider a free vortex $\theta_v = \arctan(\rho^2 y/x)$ emerging at the temperature T in a FF superfluid, the free-energy change of the system is

$$F = U_v - TS_v, \quad (\text{S37})$$

where U_v is the energy of the vortex in a system of size R

$$\begin{aligned} U_v &= \int d\mathbf{r} [J_{xx}(\partial_x \theta_v)^2 + J_{yy}(\partial_y \theta_v)^2] \\ &= \pi \sqrt{J_{xx}J_{yy}} \ln(R/a), \end{aligned} \quad (\text{S38})$$

with the size of the vortex core a . The entropy of the vortex is

$$S_v = 2\ln\left(\frac{R}{a}\right), \quad (\text{S39})$$

because the number of configurations that a vortex localizes in a system is $(R/a)^2$. Here we set $k_b = 1$. It turns out that a single vortex can be thermally excited when $F = 0$, leading to the BKT temperature

$$T_{\text{BKT}} = \frac{\pi}{2} \sqrt{J_{xx}J_{yy}}. \quad (\text{S40})$$

This is the generalized KT relation (Eq.(4) in the main text) [S5], which becomes KT relation when $J_{xx} = J_{yy}$.

S-3. BKT TEMPERATURE, SUPERFLUID DENSITY, AND SOUND SPEEDS

In the main text, we have plotted the BKT temperature, superfluid density, and sound speeds as a function of out-of-Zeeman field h_z for fixed in-plane Zeeman field h_x in Fig. 3. Here, we provide more data ($h_x = 0.2E_F$ and

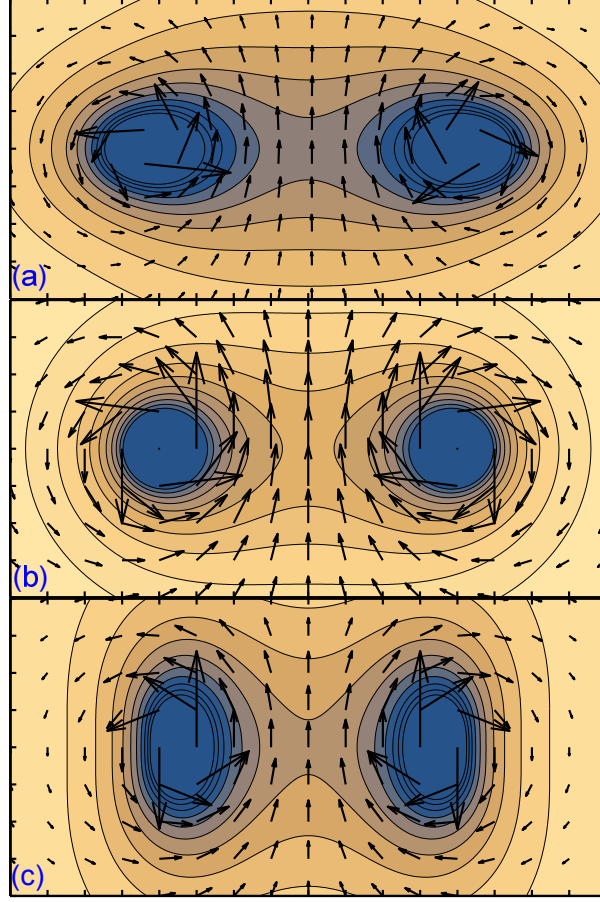


FIG. S2: (Color online) Vortex-antivortex structure for topological superfluids corresponding to $\rho_{xx} > \rho_{yy}$ in (a) with $h_z = 0.04E_F$, $\rho_{xx} = \rho_{yy}$ in (b) with $h_z = 0.6E_F$, and $\rho_{xx} < \rho_{yy}$ in (c) with $h_z = 0.8E_F$, evaluated around T_{BKT} . Here $\alpha K_F = E_F$, $E_b = 0.3E_F$, and $h_x = 0.8E_F$.

$h_x = 0.8E_F$) in Fig S1. The sound speeds are anisotropic and the one along the x direction fall quicker than those along the y direction with increasing h_z as clearly shown by the yellow lines in Fig. S1, leading to $v_y > v_x$. The reason is the symmetry restoration of the Fermi surface at large h_z , where Q_y begins decreasing, and this leads to the reverse of superfluid densities that $\rho_{xx} < \rho_{yy}$ at large h_z .

S-4. VORTEX-ANTIVORTEX VELOCITY FIELD STRUCTURE

In the main text, we have shown that anisotropic V-AV pairs emerges across the BKT temperature. The anisotropy originates from the phase field that depends on the ratio of superfluid densities along different directions. Here, to visualize V-AV pairs, we plot their velocity fields in Fig. S2. It clearly shows that there are three distinct vortex cores: elliptical with the major axis along the x direction in (a), circular in (b), and elliptical with the major axis along the y direction in (c), corresponding to $\rho_{xx} > \rho_{yy}$, $\rho_{xx} = \rho_{yy}$, and $\rho_{xx} < \rho_{yy}$ respectively. We note that although V-AV pairs have circular structure in (b), the same as traditional BCS superfluids, the superfluids have Cooper pairs with finite center-of-mass momenta.

* Corresponding Author, Email: chuanwei.zhang@utdallas.edu

[S1] Y. Xu, C. Qu, M. Gong, and C. Zhang, Phys. Rev. A **89**, 013607 (2014).

[S2] Z. Zheng, M. Gong, X. Zou, C. Zhang, and G. Guo, Phys. Rev. A **87**, 031602(R) (2013).

- [S3] Y. Xu, R.-L Chu, and C. Zhang, Phys. Rev. Lett. **112**, 136402 (2014).
 - [S4] M. Gong, G. Chen, S. Jia, and C. Zhang, Phys. Rev. Lett. **109**, 105302 (2012).
 - [S5] J. P.A. Devreese, J. Tempere, and C. A.R. Sá de Melo, arXiv:1403.5780.
 - [S6] V. L. Berezinskii, Sov. Phys. JETP **32**, 493 (1971).
 - [S7] J. M. Kosterlitz and D. Thouless, J. Phys. C **5**, L124 (1972); **6**, 1181 (1973).
-